JUSTC

Article

http://justc.ustc.edu.cn

Received: March 25, 2024; Accepted: May 08, 2024

Synergistic effect of heterogeneous single atoms and clusters for improved catalytic performance

Long Liu[1], Wenting Gao[1], Yiling Ma[1], Kainan Mei[1], Wenlong Wu[1], Hongliang Li[1], Zhirong Zhang[1] ✉, and Jie Zeng[1,2] ✉

[1]*Hefei National Research Center for Physical Sciences at the Microscale, Key Laboratory of Strongly Coupled Quantum Matter Physics of Chinese Academy of Sciences, Key Laboratory of Surface and Interface Chemistry and Energy Catalysis of Anhui Higher Education Institutes, Department of Chemical Physics, University of Science and Technology of China, Hefei 230026, China;*
[2]*School of Chemistry & Chemical Engineering, Anhui University of Technology, Ma'anshan 243002, China*

✉Correspondence: Zhirong Zhang, E-mail: zzhirong@ustc.edu.cn; Jie Zeng, E-mail: zengj@ustc.edu.cn

Graphical abstract

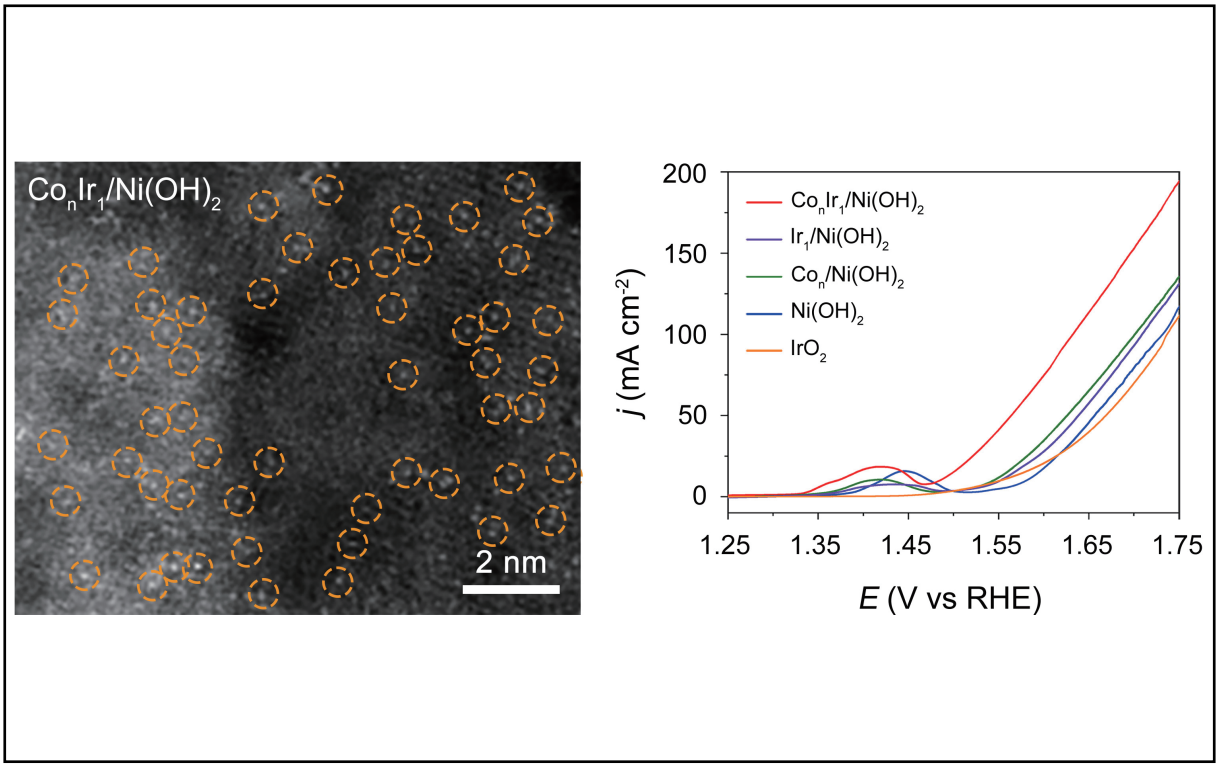

Ir single atoms and Co clusters synergistically improved the catalytic activity toward the oxygen evolution reaction.

Public summary

- A heterogeneous single-atom cluster system was constructed by anchoring Ir single atoms and Co clusters on the oxygen vacancy sites of the $Ni(OH)_2$ nanosheets.
- The Ir single atoms were mainly coordinated with oxygen, while the Co clusters were also coordinated with oxygen and formed by the second shell of the Co-Co coordination.
- Ir single atoms and Co clusters synergistically improved the catalytic activity and accelerated the kinetics of the oxygen evolution reaction.

Citation: Liu L, Gao W T, Ma Y L, et al. Synergistic effect of heterogeneous single atoms and clusters for improved catalytic performance. *JUSTC*, **2024**, 54(6): 0605. DOI: 10.52396/JUSTC-2024-0046

JUSTC

Article

http://justc.ustc.edu.cn

Received: March 25, 2024; Accepted: May 08, 2024

Synergistic effect of heterogeneous single atoms and clusters for improved catalytic performance

Long Liu[1], Wenting Gao[1], Yiling Ma[1], Kainan Mei[1], Wenlong Wu[1], Hongliang Li[1], Zhirong Zhang[1] ✉, and Jie Zeng[1,2] ✉

[1]*Hefei National Research Center for Physical Sciences at the Microscale, Key Laboratory of Strongly Coupled Quantum Matter Physics of Chinese Academy of Sciences, Key Laboratory of Surface and Interface Chemistry and Energy Catalysis of Anhui Higher Education Institutes, Department of Chemical Physics, University of Science and Technology of China, Hefei 230026, China;*
[2]*School of Chemistry & Chemical Engineering, Anhui University of Technology, Ma'anshan 243002, China*

✉Correspondence: Zhirong Zhang, E-mail: zzhirong@ustc.edu.cn; Jie Zeng, E-mail: zengj@ustc.edu.cn

Cite This: *JUSTC*, **2024**, 54(6): 0605 (7pp)

Read Online

SI Supporting Information

Abstract: Electrocatalytic water splitting provides an efficient method for the production of hydrogen. In electrocatalytic water splitting, the oxygen evolution reaction (OER) involves a kinetically sluggish four-electron transfer process, which limits the efficiency of electrocatalytic water splitting. Therefore, it is urgent to develop highly active OER catalysts to accelerate reaction kinetics. Coupling single atoms and clusters in one system is an innovative approach for developing efficient catalysts that can synergistically optimize the adsorption and configuration of intermediates and improve catalytic activity. However, research in this area is still scarce. Herein, we constructed a heterogeneous single-atom cluster system by anchoring Ir single atoms and Co clusters on the surface of $Ni(OH)_2$ nanosheets. Ir single atoms and Co clusters synergistically improved the catalytic activity toward the OER. Specifically, $Co_nIr_1/Ni(OH)_2$ required an overpotential of 255 mV at a current density of 10 mA·cm^{-2}, which was 60 mV and 67 mV lower than those of $Co_n/Ni(OH)_2$ and $Ir_1/Ni(OH)_2$, respectively. The turnover frequency of $Co_nIr_1/Ni(OH)_2$ was 0.49 s^{-1}, which was 4.9 times greater than that of $Co_n/Ni(OH)_2$ at an overpotential of 300 mV.

Keywords: single-atom cluster catalysts; synergistic effect; oxygen evolution reaction

CLC number: O643.36; TK91 **Document code:** A

1 Introduction

Hydrogen energy is clean and renewable. The widespread use of hydrogen energy can significantly reduce the reliance on fossil fuels[1–5]. Clean hydrogen energy can be obtained by electrocatalytic water splitting[6–10]. In electrocatalytic water splitting, the anodic oxygen evolution reaction (OER) involves a kinetically sluggish four-electron transfer process, which limits the efficiency of hydrogen production by electrocatalytic water splitting[11–17]. Developing efficient OER catalysts to accelerate reaction kinetics is urgent for large-scale hydrogen production[18,19]. As nonprecious metal electrocatalysts, Co-based electrocatalysts are promising for catalyzing the OER owing to their special geometric and electronic structures, but they still suffer from inadequate OER activity[20]. Consequently, it is necessary to enhance the OER activity of Co-based electrocatalysts.

Atomically dispersed catalysts, including single-atom and cluster catalysts, have drawn extensive attention due to their high atom-utilization efficiency and distinctive electronic structures[21–23]. Nevertheless, the OER performances of single-atom or cluster catalysts are not very satisfactory. Coupling single atoms and clusters in one catalyst is a powerful strategy for improving catalytic activity. Initially, the adsorption of intermediates can be optimized by the interaction between single atoms and clusters. For example, when NiN_4 metal atoms and Ni clusters were coupled on a carbon support, the interaction between them induced the preferred adsorption of oxygen intermediates[24]. In addition, after coupling single atoms and clusters, different adsorption behaviors at different sites can synergistically optimize the configuration of intermediates and promote the reaction. For instance, in the system of Rh single atoms and Ce clusters, different atoms of the N_2O intermediate were trapped by Rh single atoms and Ce clusters at the same time, which promoted the conversion of the N_2O intermediate into nitrogen[25]. Therefore, coupling single atoms and clusters in one system has great potential to improve the catalytic activity toward the OER. However, research in this area is still scarce.

In this work, we constructed a heterogeneous single-atom cluster system by anchoring Ir single atoms and Co clusters on a $Ni(OH)_2$ support. Structural characterization revealed that Ir single atoms with additional Co clusters were anchored on the oxygen vacancy sites. Electrochemical measurements indicated that single Ir atoms and Co clusters could efficiently catalyze the OER through synergistic effects. Specifically, $Co_nIr_1/Ni(OH)_2$ required an overpotential of 255 mV at a current density of 10 mA·cm^{-2}, which was much lower than those of $Co_n/Ni(OH)_2$ (315 mV) and $Ir_1/Ni(OH)_2$ (322 mV). At an overpotential of 300 mV, the turnover frequency (TOF) and mass activity (MA) of $Co_nIr_1/Ni(OH)_2$ were 0.49 s^{-1} and 3199 A·g^{-1}, respectively. Both the TOF and MA of

DOI: 10.52396/JUSTC-2024-0046
JUSTC, **2024**, 54(6): 0605

$Co_nIr_1/Ni(OH)_2$ were 4.9 times greater than those of $Co_n/Ni(OH)_2$.

2 Experimental details

2.1 Chemicals

Nickel nitrate ($Ni(NO_3)_2·6H_2O$), sodium nitrate ($NaNO_3$), cobalt nitrate hexahydrate ($Co(NO_3)_2·6H_2O$), *N*,*N*-dimethylformamide (DMF), sodium hydroxide (NaOH), and potassium hydroxide (KOH) were purchased from Shanghai Chemical Reagent Company. Iridium(IV) chloride hydrate ($IrCl_4·xH_2O$, Ir ≥56.0%) was purchased from Aladdin. Nafion was purchased from Sigma–Aldrich. All chemicals were used as received without further purification.

2.2 Synthesis of $Ni(OH)_2$

We prepared $Ni(OH)_2$ using a previously reported one-step approach with modifications[26]. Typically, a 160 mL solution of 10 mmol·L^{-1} $NaNO_3$ containing 23 vol% DMF as an inhibitor was mixed with an 80.0 mL solution containing 37.5 mmol·L^{-1} $Ni(NO_3)_2·6H_2O$, and this solution was stirred at 80 °C. Then, 0.5 mol·L^{-1} NaOH was added dropwise to maintain the solution pH at approximately 10. Afterward, the above solution was cooled to room temperature under nitrogen gas bubbling. The product was isolated by centrifugation at 12000 r/min for 3 min, followed by washing with ethanol and deionized water. Finally, the product was freeze-dried in a vacuum freeze-dryer overnight.

2.3 Synthesis of $Ir_1/Ni(OH)_2$, $Co_n/Ni(OH)_2$, and $Co_nIr_1/Ni(OH)_2$

$Ir_1/Ni(OH)_2$, $Co_n/Ni(OH)_2$, and $Co_nIr_1/Ni(OH)_2$ were synthesized by the electrochemical deposition method[27]. The electrochemical deposition was conducted in a standard three-electrode system. The as-prepared $Ni(OH)_2$ support (5 mg) was dispersed in a 1.0 mL homogeneous mixture containing equal amounts of H_2O and ethanol. Then, 80 μL of Nafion was added to the above mixture under ultrasonication to obtain a homogeneous ink. Five microliters of the above mixture was cast on a glassy carbon electrode (GCE) 3 mm in diameter for electrochemical deposition. During the process of electrochemical deposition, the potential range was from 1.25 V to 1.75 V with a sweep rate of 5 mV·s^{-1}. For electrochemical deposition, metal precursors were added to 100 mL of 1.0 mol·L^{-1} KOH electrolyte. In this process, 100 μL of 0.1 mol·L^{-1} $Co(NO_3)_2·6H_2O$ solution and 100 μL of 0.1 mol·L^{-1} $IrCl_4·xH_2O$ solution were used as the metal precursors for $Co_n/Ni(OH)_2$ and $Ir_1/Ni(OH)_2$, respectively. In the process of preparing $Co_nIr_1/Ni(OH)_2$, 100 μL of 0.1 mol·L^{-1} $Co(NO_3)_2·6H_2O$ solution was added to the electrolyte, and after the deposition of Co clusters, 100 μL of 0.1 mol·L^{-1} $IrCl_4·xH_2O$ solution was added for the electrochemical deposition of single Ir atoms. For the deposition of Co clusters, we repeated the linear sweep scan eight times, and for the deposition of single Ir atoms, we carried out the linear sweep only once.

3 Results and discussion

As stated in the experimental section, Ir single atoms and Co clusters were anchored on the surface of $Ni(OH)_2$ through an electrochemical deposition method. In the process of electrochemical deposition, Co or Ir-based anions were driven to the anode by an electric field. These metal anions might be derived from the combination of metal ions in the precursors with OH^- in the electrolyte. The formation of single atoms or clusters could be regulated by changing the number of scanning cycles. After depositing Ir single atoms and Co clusters, the $Ni(OH)_2$ support still displayed a nanosheet morphology similar to that of the original $Ni(OH)_2$, and no Co or Ir-based nanoparticles appeared in the transmission electron microscopy (TEM) images (Figs. S1a and S2). In the X-ray diffraction (XRD) patterns, all diffraction peaks were indexed to standard $Ni(OH)_2$ (PDF #74-2075), which implied the absence of Co or Ir-based nanoparticles (Figs. S1b and S3). High-angle annular dark-field scanning TEM (HAADF-STEM) was used to identify clusters and single atoms. As shown in the HAADF-STEM image of $Co_n/Ni(OH)_2$, Co clusters were not observed because the atomic number of the cobalt element was close to that of the nickel element (Fig. 1a). In the HAADF-STEM images of $Ir_1/Ni(OH)_2$ and $Co_nIr_1/Ni(OH)_2$ (Fig. 1b, c), the isolated Ir atoms were atomically dispersed on the $Ni(OH)_2$ support. Energy-dispersive X-ray (EDX) elemental mapping images were used to show the elemental distribution. Ni, O, and Co were distributed across the material according to the EDX elemental mapping images of $Co_n/Ni(OH)_2$, which suggested the existence of Co species (Fig. 1d). The EDX elemental mapping results of $Ir_1/Ni(OH)_2$ showed that Ni, O, and Ir were distributed across the material (Fig. 1e), and the EDX elemental mapping images of $Co_nIr_1/Ni(OH)_2$ also showed that Ni, O, Co, and Ir were distributed across the catalyst, which demonstrated the existence of Co and Ir species (Fig. 1f). The mass loadings of Co species in $Co_n/Ni(OH)_2$ and the mass loadings of Ir species in $Ir_1/Ni(OH)_2$ were determined to be 2.92 wt% and 2.13 wt%, respectively, by inductively coupled plasma atomic emission spectroscopy (ICP–AES). The mass loadings of Co and Ir species in $Co_nIr_1/Ni(OH)_2$ were determined to be 2.64 wt% and 2.44 wt%, respectively.

We further elucidated the electronic structure and coordination environment of the Co species on $Co_n/Ni(OH)_2$ and $Co_nIr_1/Ni(OH)_2$ and the Ir species on $Ir_1/Ni(OH)_2$ and $Co_nIr_1/Ni(OH)_2$ by X-ray absorption near-edge spectroscopy (XANES) and extended X-ray absorption fine structure (EXAFS) measurements. The Co *K*-edge XANES spectra showed that the absorption edges of $Co_n/Ni(OH)_2$ and $Co_nIr_1/Ni(OH)_2$ were slightly shifted to a higher energy than that of Co_2O_3, indicating that both the valence states of Co species for $Co_n/Ni(OH)_2$ and $Co_nIr_1/Ni(OH)_2$ were slightly greater than +3 (Fig. 2a). Moreover, the absorption edges of $Co_n/Ni(OH)_2$ and $Co_nIr_1/Ni(OH)_2$ were close, which indicated that the valence state of the Co species was not affected by the deposition of single Ir atoms. In the EXAFS spectra, there were two peaks at approximately 1.47 Å and 2.42 Å in the *R* space for both $Co_n/Ni(OH)_2$ and $Co_nIr_1/Ni(OH)_2$. The peak at approximately 1.47 Å was assigned to Co–O bonding, and the peak at 2.42 Å was assigned to Co–Co bonding. The presence of Co–Co bonds confirmed the existence of Co clusters (Fig. 2b). By fitting the experimental EXAFS spectra,

DOI: 10.52396/JUSTC-2024-0046
JUSTC, **2024**, 54(6): 0605

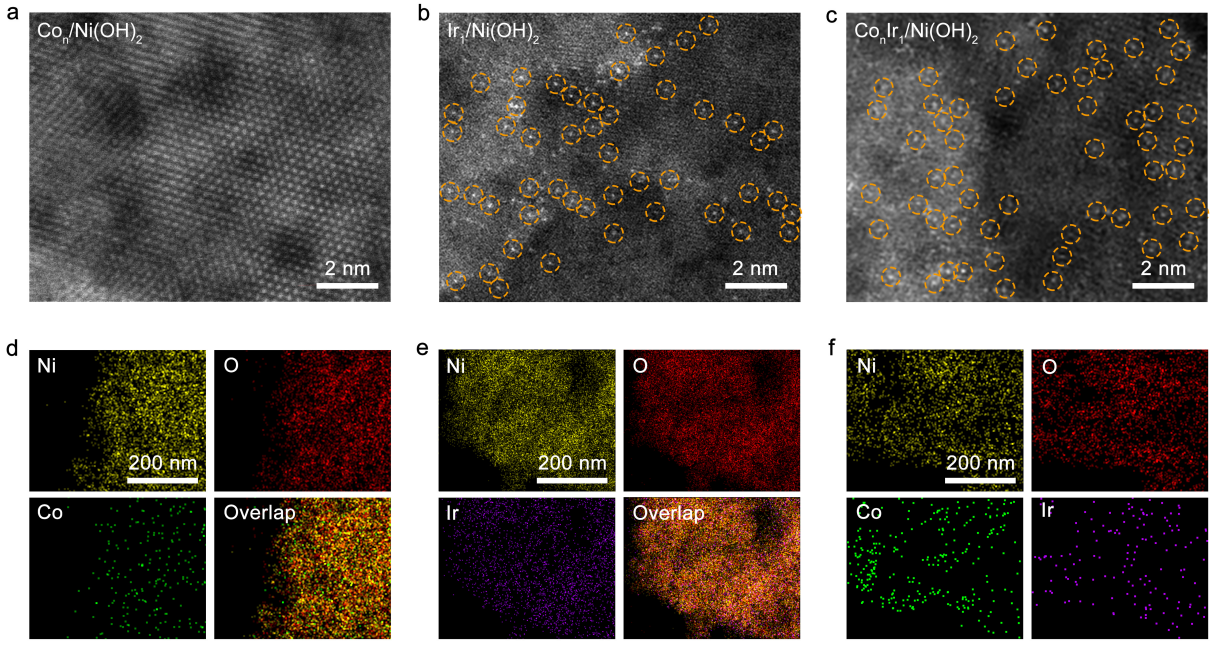

Fig. 1. Structural characterization of $Co_n/Ni(OH)_2$, $Ir_1/Ni(OH)_2$, and $Co_nIr_1/Ni(OH)_2$. HAADF-STEM images of $Co_n/Ni(OH)_2$ (a), $Ir_1/Ni(OH)_2$ (b), and $Co_nIr_1/Ni(OH)_2$ (c). EDX elemental mapping of $Co_n/Ni(OH)_2$ (d), $Ir_1/Ni(OH)_2$ (e), and $Co_nIr_1/Ni(OH)_2$ (f).

the coordination numbers of Co–O bonding were determined to be 5.69 and 5.25 for $Co_n/Ni(OH)_2$ and $Co_nIr_1/Ni(OH)_2$, respectively. The coordination numbers of the Co–O bonds suggested that Co coordinated with the hydroxygen and then was deposited on the support. The coordination numbers of Co–Co bonds were determined to be 4.02 and 2.98 for $Co_n/Ni(OH)_2$ and $Co_nIr_1/Ni(OH)_2$, respectively (Table S1). The results confirmed the presence of Co clusters. The Ir L_3-edge XANES spectra showed that the white line intensities of $Ir_1/Ni(OH)_2$ and $Co_nIr_1/Ni(OH)_2$ were slightly greater than that of IrO_2, indicating that both the valence states of Ir species for $Ir_1/Ni(OH)_2$ and $Co_nIr_1/Ni(OH)_2$ were slightly greater than +4 (Fig. 2c). In addition, the white line intensities of $Ir_1/Ni(OH)_2$ and $Co_nIr_1/Ni(OH)_2$ were similar, which indicated similar valence states of Ir species for $Ir_1/Ni(OH)_2$ and $Co_nIr_1/Ni(OH)_2$. In the EXAFS spectra, there was a peak at approximately 1.73 Å in the *R* space for both $Ir_1/Ni(OH)_2$ and $Co_nIr_1/Ni(OH)_2$. The peak at approximately 1.73 Å was assigned to Ir–O bonding, and the absence of Ir–Ir bonding confirmed the presence of single Ir atoms (Fig. 2d). The above results suggested that Ir single atoms and Co clusters were successfully deposited on the $Ni(OH)_2$ supports, that Ir single atoms were mainly coordinated with oxygen, and that Co clusters were also coordinated with oxygen and formed by the second shell of the Co-Co coordination system.

X-ray absorption spectroscopy (XAS) and X-ray photoelectron spectroscopy (XPS) were used to investigate the effects of depositing single Ir atoms on the Co clusters. In the Co *L*-edge XAS spectra of $Co_n/Ni(OH)_2$ and $Co_nIr_1/Ni(OH)_2$, there were two peaks located at 784.2 and 798.2 eV, which were assigned to the Co L_3-edge and Co L_2-edge, respectively. The peak positions of $Co_n/Ni(OH)_2$ and $Co_nIr_1/Ni(OH)_2$ were identical, suggesting no obvious change in the Co valence state after the deposition of Ir species on the surface of $Co_n/Ni(OH)_2$ (Fig. S4). XAS and XPS could also probe the effects of depositing single Ir atoms and Co clusters for support. In the Ni *L*-edge XAS spectra of $Ni(OH)_2$, $Ir_1/Ni(OH)_2$, $Co_n/Ni(OH)_2$, and $Co_nIr_1/Ni(OH)_2$, there were two peaks located at 857.2 and 874.6 eV, which were assigned to the Ni L_3-edge and Ni L_2-edge, respectively, and the similar peak positions suggested no obvious changes in the Ni valence state after the deposition of Co and Ir species on the surface of $Ni(OH)_2$ (Fig. S5). In addition, the identical peak positions in the Ni 2p XPS spectra of $Ni(OH)_2$, $Ir_1/Ni(OH)_2$, $Co_n/Ni(OH)_2$, and $Co_nIr_1/Ni(OH)_2$ were similar (Fig. S6). In the O 1s XPS spectrum, three peaks at 533.0, 531.7, and 530.8 eV corresponded to adsorbed H_2O, oxygen vacancies, and Ni-OH, respectively. After the deposition of single Ir atoms and Co clusters, the oxygen vacancy concentrations of $Ir_1/Ni(OH)_2$ and $Co_n/Ni(OH)_2$ decreased from 31.4% to 24.1% and 25.2%, respectively. This result implied that both Ir single atoms and Co clusters occupied part of the oxygen vacancy sites on the surface of $Ni(OH)_2$ (Fig. S7a–c). Similarly, the minimal oxygen vacancy concentration of $Co_nIr_1/Ni(OH)_2$ (19.2%) also implied that both Ir single atoms and Co clusters occupied part of the oxygen vacancy sites on the surface of $Ni(OH)_2$ (Fig. S7d). The XAS and XPS results indicated that Ir single atoms and Co clusters were anchored on the oxygen vacancy sites of the support and did not change the electronic structure of the support.

To verify the synergistic effect between the single Ir atoms and the Co clusters, the OER activities of $Ni(OH)_2$, $Co_n/Ni(OH)_2$, $Ir_1/Ni(OH)_2$, and $Co_nIr_1/Ni(OH)_2$ were evaluated. Polarization curves were obtained in a 1.0 mol·L^{-1} KOH electrolyte, and the current density of the catalysts was used to compare their electrocatalytic activities toward the OER. For comparison, the OER performance of commercial IrO_2 was also evaluated in 1.0 mol·L^{-1} KOH. The electrocatalytic activities of $Co_n/Ni(OH)_2$ and $Ir_1/Ni(OH)_2$ were slightly greater than that of the original $Ni(OH)_2$, but $Co_nIr_1/Ni(OH)_2$

DOI: 10.52396/JUSTC-2024-0046
JUSTC, **2024**, 54(6): 0605

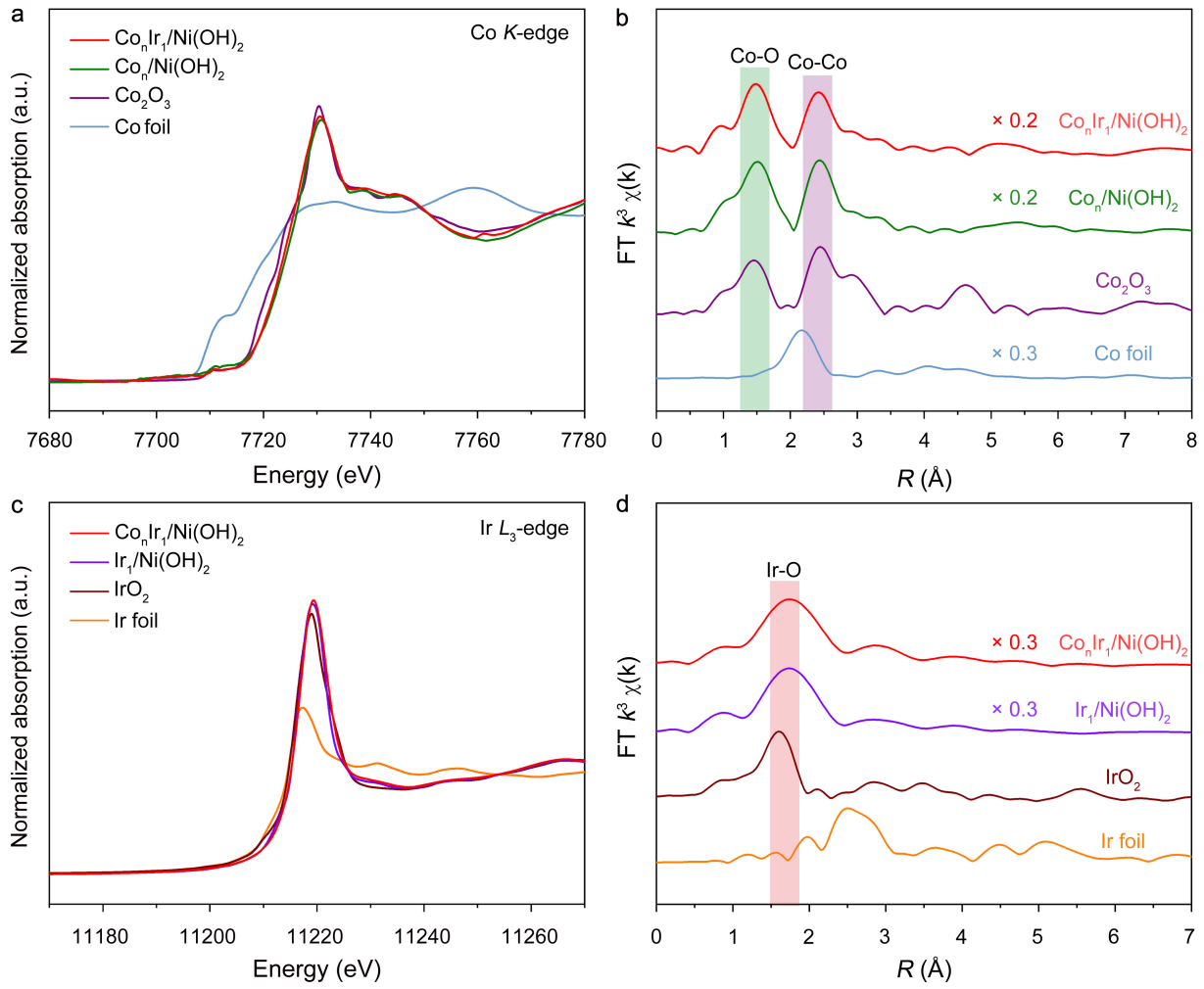

Fig. 2. Electronic structure characterization of Co clusters on $Co_n/Ni(OH)_2$ and $Co_nIr_1/Ni(OH)_2$ and Ir single atoms on $Ir_1/Ni(OH)_2$ and $Co_nIr_1/Ni(OH)_2$. Normalized XANES (a) and EXAFS (b) spectra without phase correction at the Co *K*-edge of $Co_n/Ni(OH)_2$ and $Co_nIr_1/Ni(OH)_2$. Co foil and Co_2O_3 were used as references. Normalized XANES (c) and EXAFS (d) spectra at the Ir L_3 edge of $Ir_1/Ni(OH)_2$ and $Co_nIr_1/Ni(OH)_2$. Ir foil and IrO_2 were used as references.

showed dramatically improved activity. In addition, the OER performance of $Co_nIr_1/Ni(OH)_2$ was also much better than that of IrO_2 (Fig. 3a). Specifically, $Co_nIr_1/Ni(OH)_2$ required an overpotential of 255 mV at a current density of 10 mA·cm^{-2}, which was much lower than those of $Co_n/Ni(OH)_2$ (315 mV), $Ir_1/Ni(OH)_2$ (322 mV), and IrO_2 (322 mV) (Fig. 3b). In addition, the MA and TOF were employed to investigate the intrinsic activity of $Co_n/Ni(OH)_2$ and $Co_nIr_1/Ni(OH)_2$. At an overpotential of 300 mV, the MA of $Co_nIr_1/Ni(OH)_2$ was 3199 A·g^{-1}, and the MA of $Co_n/Ni(OH)_2$ was 657 A·g^{-1} by normalizing the mass of the Co sites. In addition, the TOF of $Co_nIr_1/Ni(OH)_2$ was 0.49 s^{-1}, and the TOF of $Co_n/Ni(OH)_2$ was 0.10 s^{-1} at an overpotential of 300 mV. Both the MA and TOF of $Co_nIr_1/Ni(OH)_2$ were 4.9 times greater than those of $Co_n/Ni(OH)_2$ (Fig. 3c). For comparison, the TOF of $Co_nIr_1/Ni(OH)_2$ surpassed that of most reported Co-based OER catalysts (Fig. 3d)[28–36]. The above results revealed that Ir single atoms had poor OER activity but could synergistically catalyze the OER process with Co clusters.

The electrochemically active surface areas (ECSAs) of the catalysts were calculated to investigate the existing forms of the Ir and Co species. As shown in Fig. S8, the ECSA of $Co_n/Ni(OH)_2$ (44.79 mF·cm^{-2}) was much larger than that of $Ni(OH)_2$ (25.21 mF·cm^{-2}), which implied that the Co species were deposited as clusters. The ECSA of $Ir_1/Ni(OH)_2$ (27.12 mF·cm^{-2}) was close to that of $Ni(OH)_2$, which suggested that Ir species were deposited as single atoms. In addition, the ECSA of $Co_nIr_1/Ni(OH)_2$ (46.17 mF·cm^{-2}) was much larger than that of $Ir_1/Ni(OH)_2$ but was close to that of $Co_n/Ni(OH)_2$, which also implied that Ir and Co existed as single atoms and clusters, respectively.

To measure the intrinsic kinetic behaviors of the catalysts, the Tafel slopes of $Ni(OH)_2$, $Co_n/Ni(OH)_2$, $Ir_1/Ni(OH)_2$, and $Co_nIr_1/Ni(OH)_2$ were calculated. The Tafel slope of $Co_nIr_1/Ni(OH)_2$ was 86 mV·dec^{-1}, which was lower than those of $Ni(OH)_2$ (113 mV·dec^{-1}), $Co_n/Ni(OH)_2$ (95 mV·dec^{-1}), and $Ir_1/Ni(OH)_2$ (129 mV·dec^{-1}). To evaluate the interfacial charge-transfer resistance of these catalysts, electrochemical impedance analysis was carried out (Fig. S9). According to the electrochemical impedance spectroscopy (EIS) results, the semicircle diameter of $Co_nIr_1/Ni(OH)_2$ was the smallest among those of these catalysts, suggesting that $Co_nIr_1/Ni(OH)_2$ had the fastest charge transfer at the interface, which was conducive to OER kinetics[37]. The Tafel slopes

DOI: 10.52396/JUSTC-2024-0046
JUSTC, **2024**, 54(6): 0605

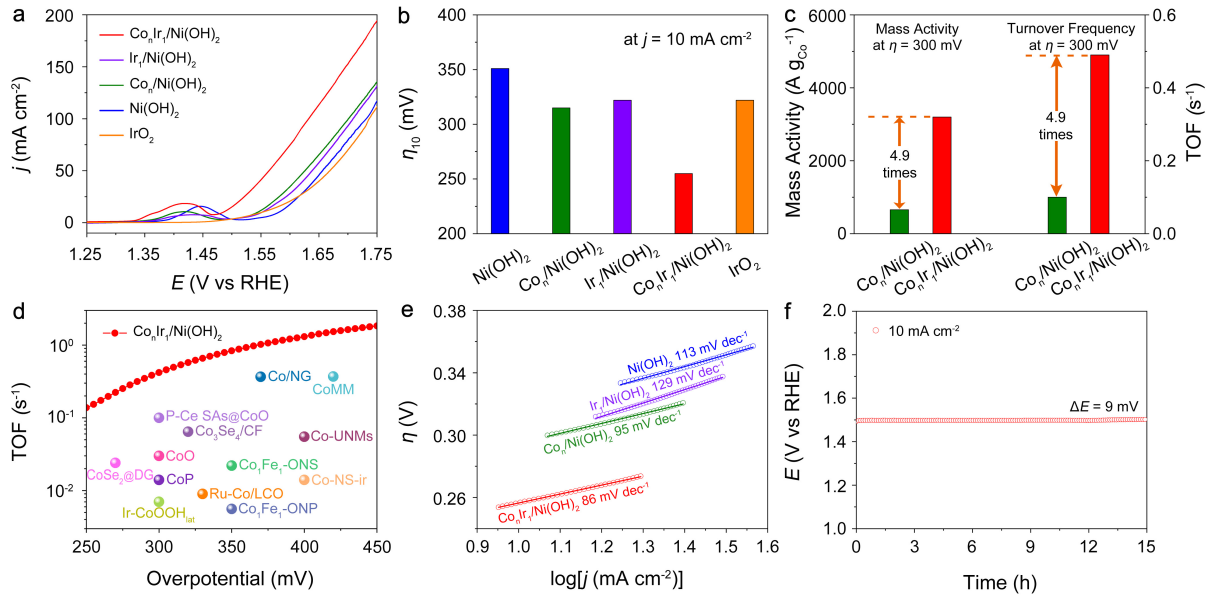

Fig. 3. Electrocatalytic performances toward the OER. (a) Polarization curves of $Ni(OH)_2$, $Co_n/Ni(OH)_2$, $Ir_1/Ni(OH)_2$, $Co_nIr_1/Ni(OH)_2$ and IrO_2. The measurements were conducted in 1.0 mol·L^{-1} KOH. (b) Overpotentials at a current density of 10 mA·cm^{-2} for $Ni(OH)_2$, $Co_n/Ni(OH)_2$, $Ir_1/Ni(OH)_2$, $Co_nIr_1/Ni(OH)_2$ and IrO_2. (c) Mass activities and turnover frequencies of $Co_n/Ni(OH)_2$ and $Co_nIr_1/Ni(OH)_2$ at an overpotential of 300 mV. (d) Comparison of the turnover frequencies of reported Co-based catalysts and $Co_nIr_1/Ni(OH)_2$ for the OER. (e) Tafel slopes of $Ni(OH)_2$, $Ir_1/Ni(OH)_2$, $Co_n/Ni(OH)_2$, and $Co_nIr_1/Ni(OH)_2$. (f) Chronopotentiometric curve of $Co_nIr_1/Ni(OH)_2$ toward the OER at a current density of 10 mA·cm^{-2} for 15 h.

and EIS results indicated that the synergy of single Ir atoms and Co clusters not only improved the catalytic activity but also accelerated the reaction kinetics.

A galvanostatic test was also conducted at a current density of 10 mA·cm^{-2} to evaluate the durability of $Co_nIr_1/Ni(OH)_2$. After 15 h, no noticeable decay in the OER activity was observed. The applied voltage of $Co_nIr_1/Ni(OH)_2$ slightly increased by 9 mV after 15 h of stability testing, demonstrating its excellent stability (Fig. 3f). The mass loadings of Co (2.62 wt%) and Ir (2.30 wt%) in $Co_nIr_1/Ni(OH)_2$ after the stability test were close to those of Co (2.64 wt%) and Ir (2.44 wt%) in the original $Co_nIr_1/Ni(OH)_2$. The results showed that Co and Ir species hardly fell off the surface of the $Ni(OH)_2$ support during the electrochemical oxygen evolution process. The morphology and structure of $Co_nIr_1/Ni(OH)_2$ were characterized after the durability test. The Ir atoms retained their isolated dispersion on the $Ni(OH)_2$ support according to the HAADF-STEM image (Fig. 4a). The Ni, O, Co, and Ir were distributed across the material without obvious aggregation, as shown by the EDX elemental mapping images (Fig. 4b). Moreover, no extra XRD diffraction peaks appeared in the XRD pattern (Fig. 4c). In the Co *L*-edge XAS spectrum, there were two peaks located at 784.2 and 798.2 eV, and the peak positions without offset suggested no obvious change in the Co valence state after the durability test (Fig. 4d). In the Ni *L*-edge XAS spectrum, there were two peaks located at 857.2 and 874.6 eV, and the identical peak positions suggested no obvious change in the Ni valence state after the durability test (Fig. 4e). In addition, the identical peak positions demonstrated a similar result in the Ni 2p XPS spectrum (Fig. 4f). In conclusion, $Co_nIr_1/Ni(OH)_2$ not only exhibited high OER activity but also achieved excellent stability.

4 Conclusions

In summary, we developed a synergistic strategy between single Ir atoms and Co clusters for promoting the OER. Both Ir single atoms and Co clusters were anchored on the oxygen vacancy sites of $Ni(OH)_2$. Due to the synergistic effect of single Ir atoms and Co clusters, $Co_nIr_1/Ni(OH)_2$ exhibited significantly improved activity and required an overpotential of 255 mV at a current density of 10 mA·cm^{-2}, which was 60 mV and 67 mV lower than those of $Co_n/Ni(OH)_2$ and $Ir_1/Ni(OH)_2$, respectively. In addition, $Co_nIr_1/Ni(OH)_2$ exhibited excellent OER intrinsic activity with a TOF of 0.49 s^{-1} at an overpotential of 300 mV. Our work not only reasonably constructed efficient catalysts for the OER but also pointed toward developing highly active catalysts.

Supporting information

The supporting information for this article can be found online at https:// doi.org/10.52396/JUSTC-2024-0046. Supplementary material (instrumentations, electrochemistry measurements) and corresponding additional data are provided in the supporting information.

Acknowledgements

This work was supported by the National Key Research and Development Program of China (2021YFA1500500, 2019YFA0405600), the CAS Project for Young Scientists in Basic Research (YSBR-051), the National Science Fund for Distinguished Young Scholars (21925204), the National Natural Science Foundation of China (22202192, U19A2015, 22221003, 22250007, 22163002), the Collaborative Innovation Program of Hefei Science Center, CAS (2022HSC-CIP004), the International Partnership, the DNL Cooperation

DOI: 10.52396/JUSTC-2024-0046
JUSTC, **2024**, 54(6): 0605

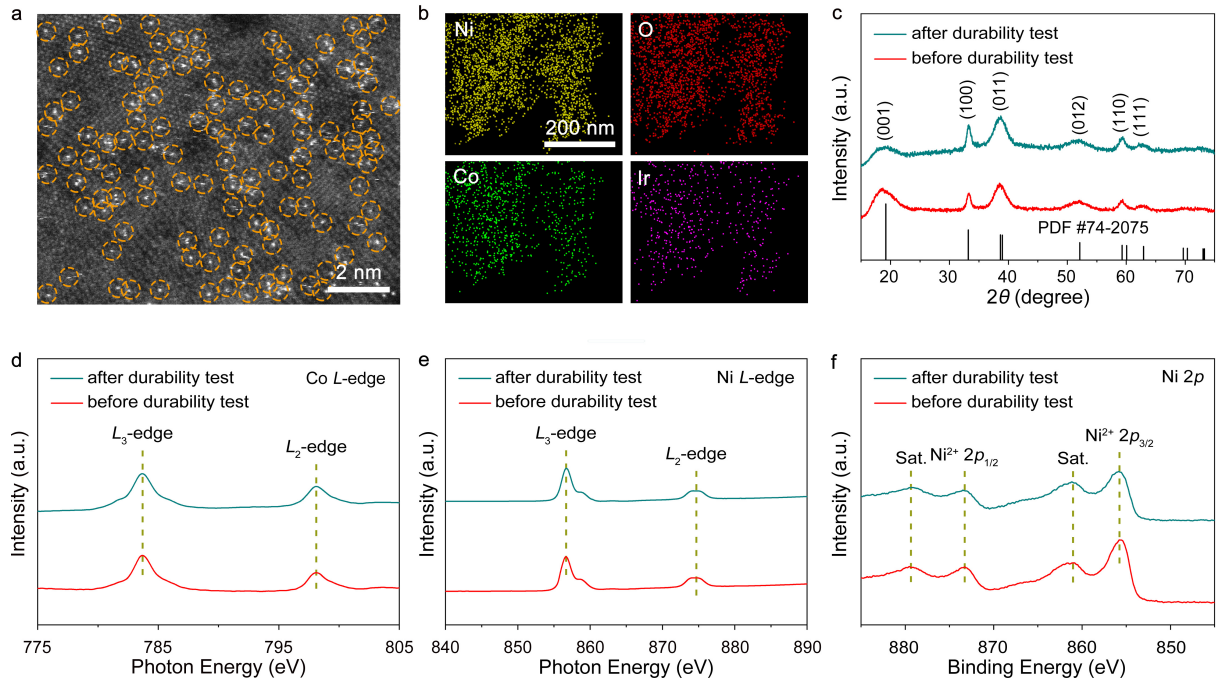

Fig. 4. Morphological and structural characterization of $Co_nIr_1/Ni(OH)_2$ after the durability test. (a) HAADF-STEM image. (b) EDX elemental mapping images. (c) XRD pattern. (d) Co *L*-edge XAS spectra. (e) Ni *L*-edge XAS spectra. (f) Ni 2p XPS spectra.

Fund, CAS (DNL202003), the USTC Research Funds of the Double First-Class Initiative (YD9990002016, YD999000-2014), the Program of Chinese Academy of Sciences (123GJHZ2022101GC), and the Fundamental Research Funds for the Central Universities (WK9990000095, WK999000-0124).

Conflict of interest

The authors declare that they have no conflict of interest.

Biographies

Long Liu is currently a graduate student in the Hefei National Research Center for Physical Sciences at the Microscale, University of Science and Technology of China, under the supervision of Prof. Jie Zeng. His research mainly focuses on the preparation of single-atom catalysts and their applications in the oxygen evolution reaction.

Zhirong Zhang is currently an Associate Professor in the Hefei National Research Center for Physical Sciences at the Microscale, University of Science and Technology of China (USTC). He received his Ph.D. degree from USTC under the tutelage of Prof. Jie Zeng in 2020. His research interests include the preparation of single-atom catalysts and their applications in electrocatalysis.

Jie Zeng is currently a Professor of Chemistry at Anhui University of Technology and Chair Professor at the University of Science and Technology of China (USTC). He received his B.S. degree from USTC in 2002 and Ph.D. degree in Condensed Matter Physics from USTC under the tutelage of Prof. Jianguo Hou and Prof. Xiaoping Wang in 2007. His research interests include selective and efficient conversion of carbon-based small molecules (such as CO, CO_2 and CH_4) to liquid fuels and high value-added chemicals from both material and mechanistic aspects.

References

[1] Chong L N, Wen J G, Song E H, et al. Synergistic Co–Ir/Ru composite electrocatalysts impart efficient and durable oxygen evolution catalysis in acid. *Advanced Energy Materials*, **2023**, *13* (37): 2302306.

[2] Lu X, Xue H, Gong H, et al. 2D layered double hydroxide nanosheets and their derivatives toward efficient oxygen evolution reaction. *Nano-Micro Letters*, **2020**, *12* (1): 86.

[3] Liao H X, Luo T, Tan P F, et al. Unveiling role of sulfate ion in nickel-iron (oxy)hydroxide with enhanced oxygen-evolving performance. *Advanced Functional Materials*, **2021**, *31* (38): 2102772.

[4] Zhang S H, Huang S C, Sun F Z, et al. Exciting lattice oxygen of nickel-iron bimetal alkoxide for efficient electrochemical oxygen evolution reaction. *Journal of Energy Chemistry*, **2024**, *88*: 194–201.

[5] Shi M M, Bao D, Yan J M, et al. Coordination and architecture regulation of electrocatalysts for sustainable hydrogen energy conversion. *Accounts of Materials Research*, **2024**, *5* (2): 160–172.

[6] Tang Y, Wu C, Zhang Q, et al. Accelerated surface reconstruction through regulating the solid-liquid interface by oxyanions in perovskite electrocatalysts for enhanced oxygen evolution. *Angewandte Chemie International Edition*, **2023**, *62* (37): e202309107.

[7] Wang X, Xi S, Huang P, et al. Pivotal role of reversible NiO_6 geometric conversion in oxygen evolution. *Nature*, **2022**, *611* (7937): 702–708.

[8] Huang Y, Jiang L W, Shi B Y, et al. Highly efficient oxygen evolution reaction enabled by phosphorus doping of the Fe electronic structure in iron-nickel selenide nanosheets. *Advanced Science*, **2021**, *8* (18): 2101775.

[9] Zeng S P, Shi H, Dai T Y, et al. Lamella-heterostructured nanoporous bimetallic iron-cobalt alloy/oxyhydroxide and cerium oxynitride electrodes as stable catalysts for oxygen evolution. *Nature Communications*, **2023**, *14* (1): 1811.

[10] Xin S S, Tang Y, Jia B H, et al. Coupling adsorbed evolution and lattice oxygen mechanism in Fe-$Co(OH)_2/Fe_2O_3$ heterostructure for enhanced electrochemical water oxidation. *Advanced Functional Materials*, **2023**, *33* (45): 2305243.

[11] Liu H, Zhang T F, Cui D, et al. Defective ferrocene-based metal–organic frameworks for efficient solar-powered water

DOI: 10.52396/JUSTC-2024-0046
JUSTC, **2024**, 54(6): 0605

oxidation via the ligand competition and etching effect. *Journal of Colloid and Interface Science*, **2024**, *657*: 664–671.
[12] Wu H, Huang Q X, Shi Y Y, et al. Electrocatalytic water splitting: Mechanism and electrocatalyst design. *Nano Research*, **2023**, *16* (7): 9142–9157.
[13] Iqbal S, Safdar B, Hussain I, et al. Trends and prospects of bulk and single-atom catalysts for the oxygen evolution reaction. *Advanced Energy Materials*, **2023**, *13* (17): 2203913.
[14] Zhang N, Du J Y, Zhou N, et al. High-valence metal-doped amorphous IrO_x as active and stable electrocatalyst for acidic oxygen evolution reaction. *Chinese Journal of Catalysis*, **2023**, *53*: 134–142.
[15] Zhao F Z, Mao X Y, Zheng X, et al. Roles of the self-reconstruction layer in the catalytic stability of a NiFeP catalyst during the oxygen evolution reaction. *Journal of Materials Chemistry A*, **2023**, *11* (1): 276–286.
[16] Chang J W, Zhang Q, Yu J K, et al. A Fe single atom seed-mediated strategy toward Fe_3C/Fe–N–C catalysts with outstanding bifunctional ORR/OER activities. *Advanced Science*, **2023**, *10* (22): 2301656.
[17] Seitz L C, Dickens C F, Nishio K, et al. A highly active and stable IrO_x/$SrIrO_3$ catalyst for the oxygen evolution reaction. *Science*, **2016**, *353* (6303): 1011–1014.
[18] Bai X F, Zhang X P, Sun Y J, et al. Low ruthenium content confined on boron carbon nitride as an efficient and stable electrocatalyst for acidic oxygen evolution reaction. *Angewandte Chemie International Edition*, **2023**, *62* (38): e202308704.
[19] Zheng Y R, Vernieres J, Wang Z B, et al. Monitoring oxygen production on mass-selected iridium–tantalum oxide electrocatalysts. *Nature Energy*, **2022**, *7* (1): 55–64.
[20] Ma Y D, Zhang H, Xia J, et al. Reduced $CoFe_2O_4$/graphene composite with rich oxygen vacancies as a high efficient electrocatalyst for oxygen evolution reaction. *International Journal of Hydrogen Energy*, **2020**, *45* (19): 11052–11061.
[21] Cao D, Wang J Y, Xu H X, et al. Construction of dual-site atomically dispersed electrocatalysts with Ru-C_5 single atoms and Ru-O_4 nanoclusters for accelerated alkali hydrogen evolution. *Small*, **2021**, *17* (31): 2101163.
[22] He T W, Santiago A R P, Kong Y C, et al. Atomically dispersed heteronuclear dual-atom catalysts: a new rising star in atomic catalysis. *Small*, **2022**, *18* (12): 2106091.
[23] Zheng X B, Li B B, Wang Q S, et al. Emerging low-nuclearity supported metal catalysts with atomic level precision for efficient heterogeneous catalysis. *Nano Research*, **2022**, *15* (9): 7806–7839.
[24] Wang Z, Jin X Y, Xu R J, et al. Cooperation between dual metal atoms and nanoclusters enhances activity and stability for oxygen reduction and evolution. *ACS Nano*, **2023**, *17* (9): 8622–8633.
[25] Chen J J, Wang S D, Li Z Y, et al. Selective reduction of NO into N_2 catalyzed by Rh_1-doped cluster anions $RhCe_2O_{3\text{-}5}^-$. *Journal of the American Chemical Society*, **2023**, *145* (33): 18658–18667.
[26] Lee S, Bai L, Hu X. Deciphering iron-dependent activity in oxygen evolution catalyzed by nickel–iron layered double hydroxide. *Angewandte Chemie International Edition*, **2020**, *59* (21): 8072–8077.
[27] Zhang Z R, Feng C, Liu C X, et al. Electrochemical deposition as a universal route for fabricating single-atom catalysts. *Nature Communications*, **2020**, *11* (1): 1215.
[28] Yu J, Li Z, Liu T, et al. Morphology control and electronic tailoring of Co_xA_y (A = P, S, Se) electrocatalysts for water splitting. *Chemical Engineering Journal*, **2023**, *460*: 141674.
[29] Zhuang L, Ge L, Yang Y, et al. Ultrathin iron-cobalt oxide nanosheets with abundant oxygen vacancies for the oxygen evolution reaction. *Advanced Materials*, **2017**, *29* (17): 1606793.
[30] Zheng X B, Yang J R, Xu Z F, et al. Ru–Co pair sites catalyst boosts the energetics for the oxygen evolution reaction. *Angewandte Chemie International Edition*, **2022**, *61* (32): e202205946.
[31] Li W, Gao X, Xiong D, et al. Hydrothermal synthesis of monolithic Co_3Se_4 nanowire electrodes for oxygen evolution and overall water splitting with high efficiency and extraordinary catalytic stability. *Advanced Energy Materials*, **2017**, *7* (17): 1602579.
[32] Yan L T, Cao L, Dai P C, et al. Metal-organic frameworks derived nanotube of nickel–cobalt bimetal phosphides as highly efficient electrocatalysts for overall water splitting. *Advanced Functional Materials*, **2017**, *27* (40): 1703455.
[33] Li M, Wang X, Liu K, et al. Reinforcing Co–O covalency via Ce(4f)–O(2p)–Co(3d) gradient orbital coupling for high-efficiency oxygen evolution. *Advanced Materials*, **2023**, *35* (30): 2302462.
[34] Feng C, Zhang Z R, Wang D D, et al. Tuning the electronic and steric interaction at the atomic interface for enhanced oxygen evolution. *Journal of the American Chemical Society*, **2022**, *144* (21): 9271–9279.
[35] Kumar P, Kannimuthu K, Zeraati A S, et al. High-density cobalt single-atom catalysts for enhanced oxygen evolution reaction. *Journal of the American Chemical Society*, **2023**, *145* (14): 8052–8063.
[36] Li Y, Li F M, Meng X Y, et al. Ultrathin Co_3O_4 nanomeshes for the oxygen evolution reaction. *ACS Catalysis*, **2018**, *8* (3): 1913–1920.
[37] Hou Y, Zuo F, Dagg A, et al. A three-dimensional branched cobalt-doped α-Fe_2O_3 nanorod/$MgFe_2O_4$ heterojunction array as a flexible photoanode for efficient photoelectrochemical water oxidation. *Angewandte Chemie International Edition*, **2013**, *52* (4): 1248–1252.

DOI: 10.52396/JUSTC-2024-0046
JUSTC, **2024**, 54(6): 0605